Miner Deposita (2018) 53:311–322
DOI 10.1007/s00126-017-0740-x

ARTICLE

Multiple episodes of mineralization revealed by Re-Os molybdenite geochronology in the Lala Fe-Cu deposit, SW China

Zhimin Zhu[1] · **Hongqi Tan**[1] · **Yingdong Liu**[1] · **Chao Li**[2]

Received: 1 April 2017 / Accepted: 17 April 2017 / Published online: 19 May 2017

Abstract The Lala Fe-Cu deposit is one of the largest iron oxide-copper-gold (IOCG) deposits in the Kangdian copper belt, southwest China. The paragenetic sequence of the Lala deposit includes six hydrothermal stages: pre-ore pervasive Na alteration (I); magnetite stage with K-feldspar and apatite (II); polymetallic disseminated/massive magnetite-sulfide stage (III); banded magnetite-sulfide stage (IV); sulfide vein stage (V); and late quartz-carbonate vein stage (VI). Fifteen molybdenite separates from stages III to VI were analyzed for Re-Os dating. Our new Re-Os data, together with previous studies, identify four distinct hydrothermal events at the Lala deposit. Molybdenite from the stage III disseminated to massive chalcopyrite-magnetite ores yielded a weighted average Re-Os age of 1306 ± 8 Ma (MSWD = 1.1, n = 6) which represents the timing of main ore formation. Molybdenite from the stage IV-banded magnetite-chalcopyrite ores yielded a weighted average Re-Os age of 1086 ± 8 Ma (MSWD = 2.2, n = 7), i.e., a second ore-forming event. Molybdenite from the stage V sulfide veins yielded a weighted average Re-Os age of 988 ± 8 Ma (MSWD = 1.3, n = 7) which represents the timing of a third hydrothermal event. Molybdenite from the quartz-carbonate veins (stage VI) yielded a weighted average Re-Os age at 835 ± 4 Ma (MSWD = 0.66, n = 10) and documented the timing of a late hydrothermal event. Our results indicate that the Lala deposit formed during multiple, protracted mineralization events over several hundred million years. The first three Mesoproterozoic mineralization events are coeval with intra-continental rifting (breakup of the supercontinent Nuna) and share a temporal link to other IOCG-style deposits within the Kangdian Copper Belt, and the last Neoproterozoic hydrothermal event is coeval with the Sibao orogeny which culminated with the amalgamation of the Yangtze Block with the Cathaysia Block at 860–815 Ma.

Keywords Fe oxide-Cu-Au deposit · Multiple episodes of mineralization · Molybdenite Re-Os dating · Lala deposit

Editorial handling: B. Lehmann

✉ Zhimin Zhu
zhu-zhimin@163.com

[1] Institute of Multipurpose Utilization of Mineral Resources, Chinese Academy of Geological Sciences, Chengdu 610041, China

[2] National Research Center for Geoanalysis, Chinese Academy of Geological Sciences, Beijing 100037, China

Introduction

Iron oxide-copper-gold (IOCG) deposits are characterized by abundant low-Ti iron oxide (magnetite and hematite), pervasive hydrothermal alkali (Na/Ca/K) alteration, and an extensional tectonic setting (Hitzman et al. 1992). As these deposits host large resources of uranium, copper, and gold, they have become important exploration targets during the past decades (Hitzman and Valenta 2005; Sillitoe 2012; Zhu 2016).

Although several authors have attempted to establish a general ore deposit model (e.g., Williams et al. 2005; Groves et al. 2010; Porter 2010; Barton 2014), much controversy remains on the genesis of these deposits. For the IOCG deposits in the Gawler craton of South Australia, a fairly restricted episode of mineralization between ~1570 and ~1600 Ma was proposed, related to the magmatism of the Hiltaba Suite and Gawler Range Volcanics (Skirrow et al. 2007). However, in most other areas, protracted mineralization seems to be critical for the formation of IOCG deposits (Barton 2014). The two competing models mainly reflect the inability to accurately and precisely determine the mineralization age of IOCG deposits. In addition, most Precambrian IOCG provinces were affected by

multiple tectonothermal events (Barton 2014). Thus, a precise chronometer for IOCG deposits resistant to thermal disturbance is required. Molybdenite usually has high Re and low Os concentrations and can resist high-grade thermal metamorphism (Stein et al. 2001; Stein 2014), which makes it a suitable mineral for dating IOCG mineralization, but the rare occurrence of molybdenite in most IOCG deposits limits its utilization (e.g., Requia et al. 2003; De Haller et al. 2006; Skirrow et al. 2007; Moreto et al. 2015b).

The Lala copper deposit is one of the largest IOCG deposits in the Kangdian copper belt, southwest China, containing 163 Mt ores (@14.4% Fe, 1.02% Cu, 0.02% Mo, 0.17 g/t Au; Zhu et al. 2013; Zhu 2016 and several unpublished reports). During recent fieldwork, we identified three textual types of Mo mineralization in the Lala deposit, i.e., disseminated to massive molybdenite, spotted-patchy molybdenite associated to chalcopyrite-quartz veins in albitite, and late molybdenite in quartz-carbonate veins. Here, we report Re-Os molybdenite ages for each of the three textural molybdenite types, which together with previously reported Re-Os data on banded molybdenite (Chen and Zhao 2012), to constrain the formation of the Lala deposit by multiple episodes of mineralization. We further propose a temporal link between the multiple episodes of mineralization of the Kangdian Copper Belt and the breakup of the supercontinent Nuna.

Geologic setting

The South China Block consists of the ~3.3–2.9 Ga Yangtze Block to the northwest and the ~2.5 Ga Cathaysia Block to the southeast (Fig. 1a). The two blocks consolidated around 860–815 Ma (i.e., Sibao orogeny or Jiangnan orogeny; Li et al. 1995, 2002; Zhao and Zhou 2011; Wang et al. 2007b; Yang et al. 2012; Yao et al. 2014; Zhao 2015). The Yangtze Block has a sparse Archean basement in the northern margin and a widespread Paleoproterozoic folded basement in the western margin (Fig. 1b), whereas the Cathaysia Block has a sparse Paleoproterozoic basement in the northeastern sector but a widespread Neoproterozoic basement in the northern sector (Zhao and Cawood 2012). The Proterozoic strata are unconformably overlain by an unmetamorphosed late Sinian to Cenozoic cover sequence (Yan et al. 2003). The Sibao orogeny resulted in widespread deformation, uplift, and upper greenschist to lower amphibolite facies metamorphism at 860–815 Ma in the Yangtze and Cathaysia Blocks (Li et al. 2002).

The Kangdian Copper Belt is a newly defined world-class IOCG metallogenic province, which extends ~300 km from SW China to N Vietnam in the west margin of the Yangtze Block (Fig. 1b, Greentree 2007; Zhao and Zhou 2011). There are more than 50 IOCG deposits hosted in the late Paleoproterozoic (1.7–1.6 Ga) meta-volcanic and meta-sedimentary sequences, and six large Fe-Cu deposits include the Lala, Xikuangshan, Yinachang, Etouchang, Dahongshan, and Sin Quyen deposits (Zhou et al. 2014). Traditionally, these deposits were thought to be syngenetic volcanogenic massive sulfide (VMS) deposits based on their ore texture and marine volcanic host rock (~1.7–1.6 Ga; Li et al. 1988). Recently, they were thought to be epigenetic IOCG deposits due to abundant low-Ti hydrothermal magnetite, elevated REE and Mo, extensive albite and K-feldspar alteration, and disseminated to massive and veined ores with local hydrothermal breccias (Zhao and Zhou 2011).

The Kangdian Copper Belt contains Proterozoic volcano-sedimentary sequences including the late Paleoproterozoic Hekou, Dahongshan, and Dongchuan Groups (~1.7–1.6 Ga; Greentree and Li 2008; Zhao et al. 2010; Zhao and Zhou 2011; Zhu et al. 2013), and the late Mesoproterozoic–early Neoproterozoic Huili and Kunyang Groups (~1.4–1.0 Ga; Greentree et al. 2006; Geng et al. 2007; Yin et al. 2011; Wang et al. 2012; Chen et al. 2014). These Proterozoic sequences were intruded by Paleoproterozoic (~1.65 Ga) and Neoproterozoic (~860–740 Ma) mafic–felsic intrusions (Zhou et al. 2014). The Sibao orogeny (860–815 Ma) resulted in upper greenschist-lower amphibolite facies metamorphism in the late Paleoproterozoic Hekou, Dahongshan, and Dongchuan Groups, whereas lower greenschist facies metamorphic overprint is visible in the late Mesoproterozoic–early Neoproterozoic Huili and Kunyang Groups.

The Lala Fe-Cu deposit is located in the north of the Kangdian Copper Belt and has six main mining sites including Luodang, Hongnipo, Laoyanghantan, Shilong, Changpuqing, and Laohushan (Fig. 2 and Table 1). The detailed geology of the Lala copper deposit has been described by Chen and Zhou (2012) and Zhu and Sun (2013). The Lala deposit is hosted by the Paleoproterozoic meta-volcano-sedimentary sequences of the Hekou Group (zircon U-Pb depositional age of 1669 ± 6 Ma, Zhu et al. 2013). The Hekou Group is in fault contact with the Huili Group (1.4–1.0 Ga) and is unconformably overlain by the Triassic Baiguowan Formation. The Hekou Group comprises the Baiyunshan and Luodang Formations from the base upward (Fig. 2). The Baiyunshan Formation consists of coarse- to fine-grained siliciclastic and carbonate rocks, whereas the Luodang Formation consists of sodic lava and pyroclastic rocks (Zhu et al. 2013).

The orebodies of the Lala deposit occur principally as stratiform, stratoid, and lentoid in accordance with the strike of host rocks and locally occur as veins crosscutting the host rocks. The host rocks are mainly biotite quartz schist, two-mica quartz schist, garnet-biotite quartz schist, and magnetite-quartz albitite of the Luodang Formation and are locally intruded by a diabase-gabbro dike (zircon U-Pb: 1657 ± 21 Ma; Chen et al. 2013b) and granite porphyry (zircon U-Pb: 1657 ± 15 Ma; Song 2014). The diabase-gabbro dike

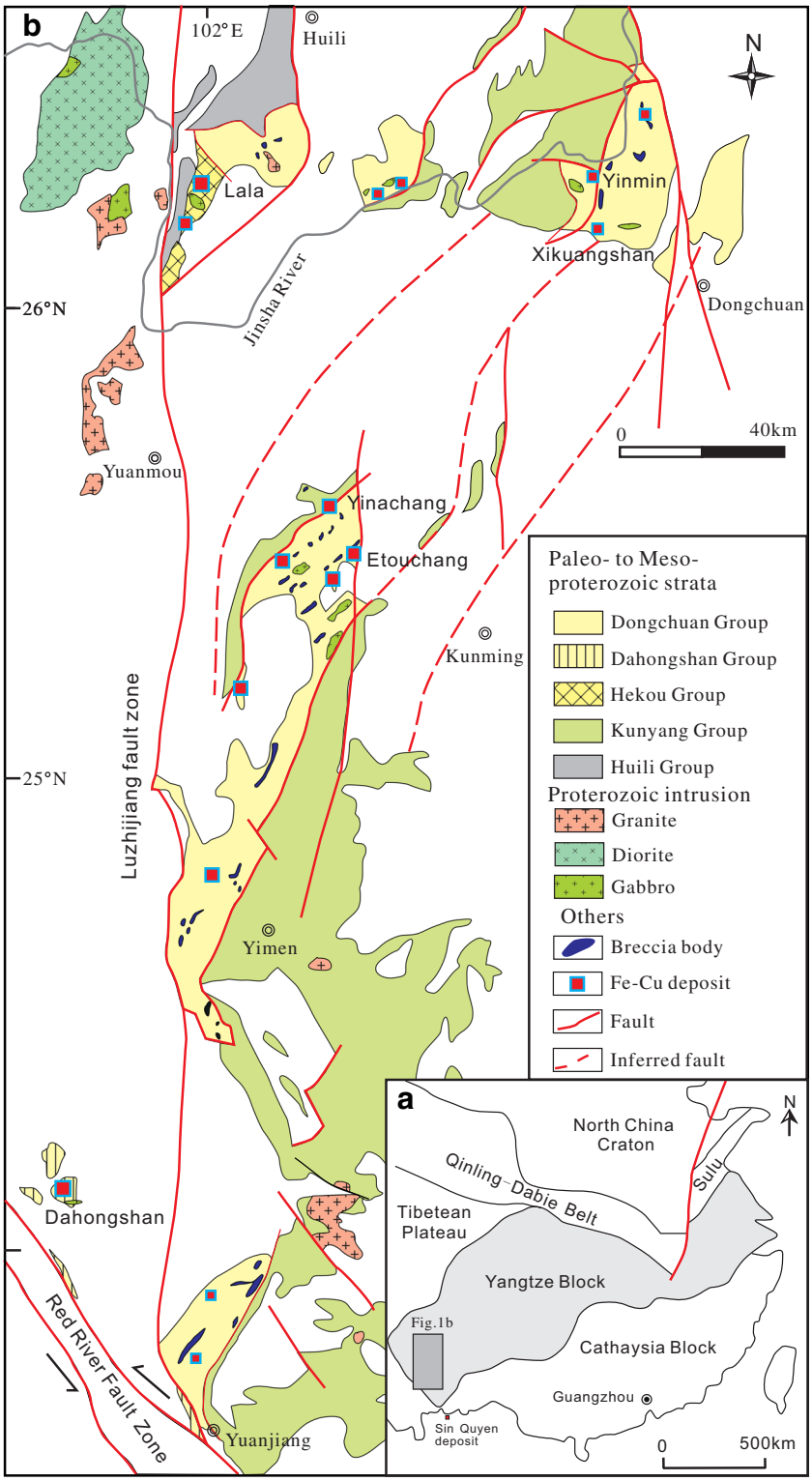

Fig. 1 **a** Simplified tectonic map showing the study area in the Yangtze Block. **b** Regional geologic map of the Kangdian Copper Belt showing major Fe-Cu deposits, Precambrian strata and plutons (modified from Zhao and Zhou 2011)

and granite porphyry are all hydrothermally altered but without clear relationship with orebodies. Locally, breccias occur in the Lala deposit and are generally associated with orebodies. The clasts of breccias are pink with low roundness and mainly consist of albite, whereas the matrices of the breccias consist of biotite and chlorite largely replaced by chalcopyrite and pyrite. Most breccias are deformed and predated metamorphism (Chen and Zhou 2012). Both orebodies and their host rock underwent greenschist-facies metamorphism at 860–815 Ma

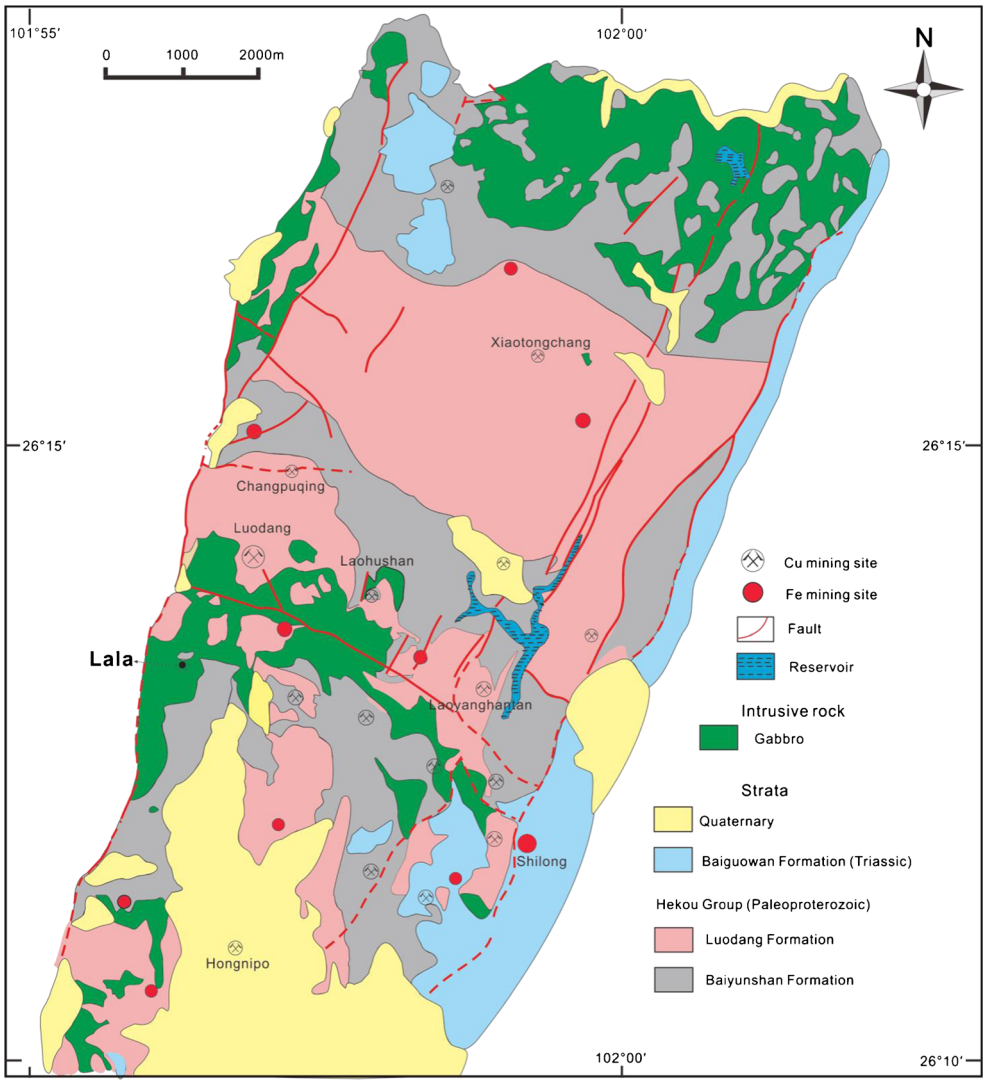

Fig. 2 Geological map of the Lala area showing the main mining sites

(Greentree 2007; Zhou et al. 2014) and were foliated and folded along NS-trending axes and cut by later north-northwest faults.

The paragenetic sequence includes six stages based on the macro- and micro-textural relationships of mineral assemblages of different ores from the Lala deposit (Zhu et al. 2009; Chen and Zhou 2012; Song 2014; and this study) (Fig. 3). Mineral assemblages of stage I to stage V are foliated and metamorphosed, whereas mineral assemblages of stage VI are unmetamorphosed. Stage I (pre-ore pervasive Na alteration) consists mainly of albite and minor amphibole, tourmaline and/or scapolite replacing the host rocks. Stage II

Table 1 Tonnages and grades of six main mining sites of the Lala deposit

Mining sites	Ore elements	Tonnage (Mt)	Fe (wt%)	Cu (wt%)	Au (g/t)	Ag (g/t)	Co (wt%)	Mo (wt%)	REE (wt%)
Luodang	Fe, Cu, Au, Ag,Co, Mo, REE	73.60	15.28	0.83	0.16	1.87	0.02	0.03	0.14
Hongnipo	Fe, Cu, Au, Ag, Co, Mo	44.37	9.31	1.42	0.10	2.39	0.01	0.01	ND
Laoyanghantan	Fe, Cu, Au, Ag, Co, Mo	29.10	12.09	1.03	0.29	2.41	0.02	0.02	ND
Shilong	Fe, Cu	9.65	38.25	0.84	ND	ND	ND	ND	ND
Changpuqing	Fe, Cu	4.33	ND	0.70	ND	ND	ND	ND	ND
Laohushan	Fe, Cu	1.84	ND	0.73	ND	ND	ND	ND	ND

Notes: Reserve and grade data are updated from several unpublished reports; *ND* is no data available

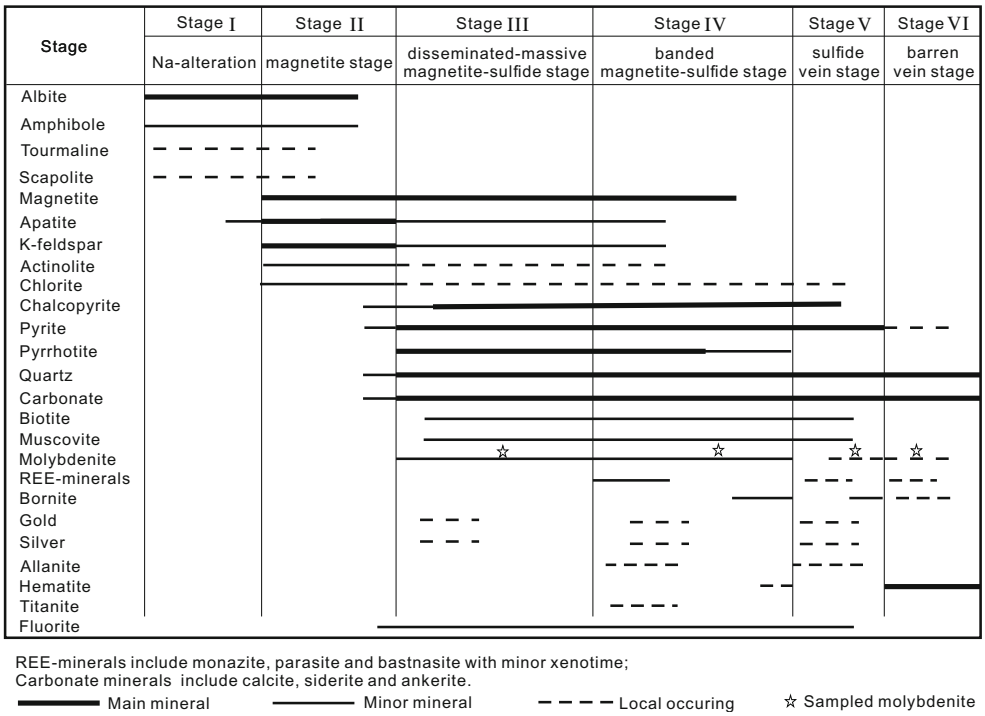

Fig. 3 Paragenetic sequence of mineralization and alteration in the Lala deposit (compiled from Zhu et al. 2009; Chen and Zhou 2012; Song 2014 and this study)

(magnetite stage) comprises magnetite, K-feldspar, and apatite, and minor actinolite and chlorite with sparse disseminated chalcopyrite and pyrite. Stage III (polymetallic-disseminated/massive magnetite-sulfide stage) is characterized by abundant magnetite, chalcopyrite, pyrite, pyrrhotite, carbonate minerals, and quartz with minor molybdenite, fluorite, apatite, K-feldspar, biotite, and muscovite; native gold and silver occur locally. Stage IV (banded magnetite-sulfide stage) has a mineral assemblage of oriented pyrite-chalcopyrite-molybdenite, magnetite, carbonate minerals, REE minerals, and quartz with local bornite, native gold, native silver, hematite, titanite, and allanite. Stage V (sulfide vein stage) is dominated by chalcopyrite, pyrite, carbonate, and quartz with variable biotite, muscovite, fluorite, pyrrhotite, bornite, molybdenite, native gold, silver, and REE minerals. The final quartz-carbonate vein stage (stage VI) has minor molybdenite and displays extensive hematite alteration in the country rocks; REE minerals and pyrite occur locally. The sulfide veins of stage V crosscut the host rocks and Fe-Cu ores of stage II to stage IV, whereas the late quartz-carbonate veins of stage VI crosscut host rocks and Fe-Cu ores of stage II to stage V. Iron ore mineralization predominantly occurs as massive and disseminated oxide and oxide-sulfide assemblages in stages II, III, and IV, whereas Cu-Mo sulfide mineralization primarily occurs as disseminated-massive and banded sulfides of stages III and IV, with minor sulfide veining in stage V. Therefore, the disseminated to massive ores of stage III and banded ores of stage IV represent the principal IOCG mineralization, the veined ores of stage V represent minor IOCG mineralization, and the veins of stage VI represent hydrothermal overprint or metamorphic remobilization.

Sampling and analytical methods

In the Lala deposit, molybdenite is present in four paragenetic stages: (1) Stage III fine-grained molybdenite distributed within disseminated to massive magnetite-chalcopyrite-pyrite ore (Fig. 4d–f), (2) stage IV molybdenite-chalcopyrite bands up to several millimeters thick (Fig. 4g–i), (3) stage VI fine-grained molybdenite within late quartz-carbonate veins with the width of several to 20 cm in thickness (Fig. 4h–i), and (4) sparse stage V coarse-grained (~2–8 mm) spotted-patchy molybdenite in sulfide-quartz veins associated with quartz albitite (Fig. 4g). Fifteen samples, with five replicates (0308-1-2, 0308-2-2, 0101-1-2, 0101-2-2, 0109-2), were collected from the Luodang open-pit in the Lala deposit for Re-Os molybdenite geochronology. The samples include nine stage VI vein stage samples (0102–0110), four stage III disseminated to massive samples (0308-1–0308-4), and two stage V spotted-patchy samples (0101-1 and 0101-2).

Molybdenite Re-Os isotope analyses were carried out in the Re-Os Laboratory, National Research Center of Geoanalysis, Chinese Academy of Geological Sciences (CAGS, Beijing). All molybdenite separates were produced and analyzed using the procedures described by Du et al. (2004). About ~0.001 to 0.05 g separates were crushed and ground to less than 200 mesh. Precisely weighed powders

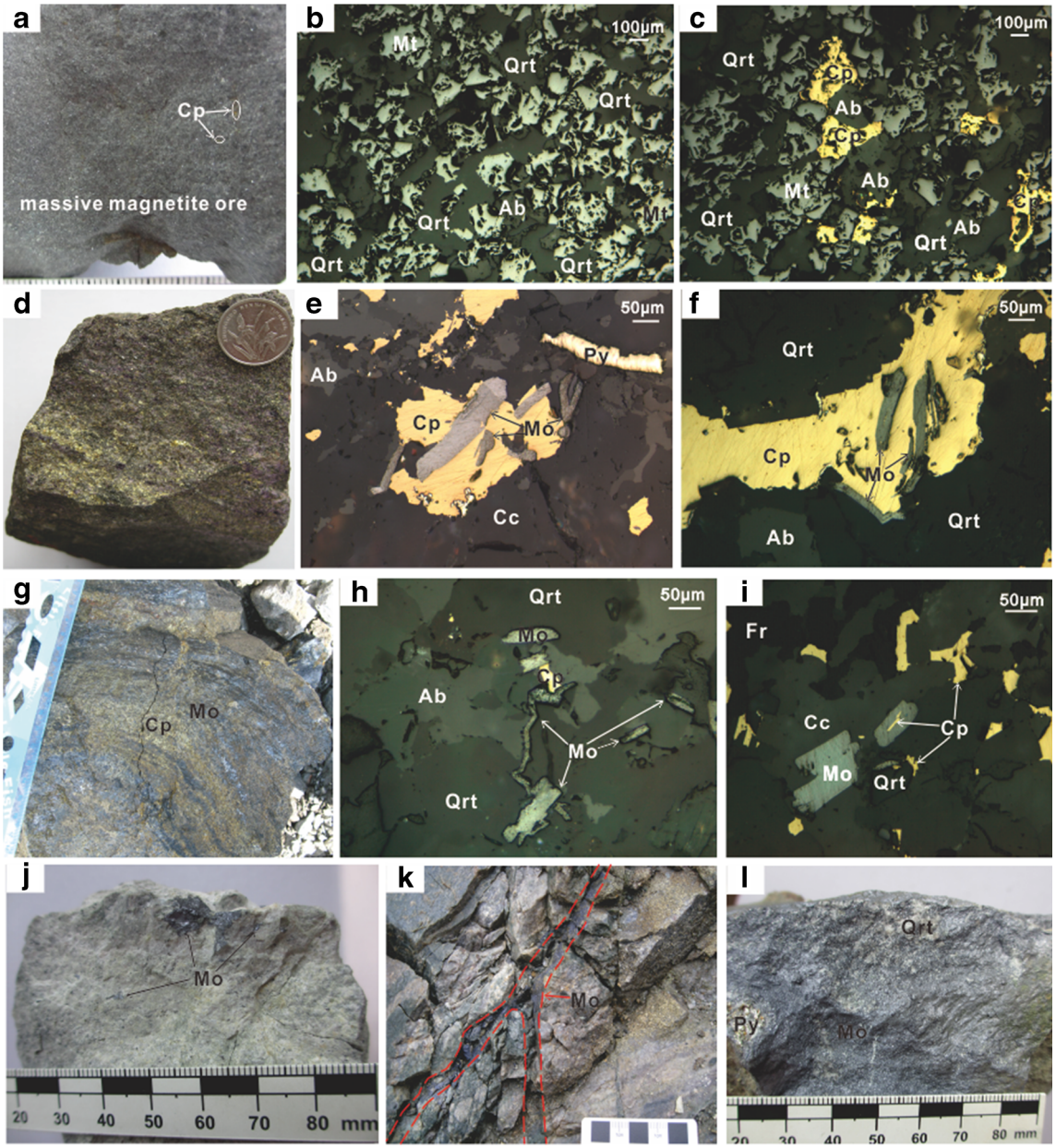

Fig. 4 Photographs of four types of molybdenite samples from the Lala deposit (**a**–**c**). Massive magnetite ore (stage II) (**d**–**f**). Disseminated to massive Cu-Mo ore (stage III). Chalcopyrite replaces molybdenite and some chalcopyrite overgrows molybdenite (**g**–**i**). Banded Cu-Mo ore (stage IV): chalcopyrite replaces molybdenite and molybdenite overgrows chalcopyrite (**j**). Spotted-patchy molybdenite ore (stage V): molybdenite in quartz albitite (**k**–**l**). Molybdenite-quartz vein (stage VI): late molybdenite-quartz-carbonate vein crosscutting the disseminated-massive Cu ores. Mineral abbreviations: *Cp* chalcopyrite, *Mo* molybdenite, *Mt* magnetite, *Py* pyrite, *Qrt* quartz, *Ab* albite, *Cc* calcite, *Fr* fluorite

were loaded into Carius tubes, together with ^{185}Re and ^{190}Os mixed spikes, and digested by reverse aqua regia. The tube was heated in an oven at 200 °C for about 24 h. Upon cooling, the bottom part of the tube was kept frozen, the neck of the tube was broken, and the contents were poured into a distillation flask and the residue was washed out with 40 ml of MQ water. Osmium was separated as OsO_4 by distillation at 105–110 °C and was trapped by Milli-Q water. During distillation, the reverse aqua regia acted as oxidizer. The residual Re-bearing solution was saved in a 150-ml Teflon beaker for Re separation. The Os isotope ratio was determined using an inductively coupled plasma mass spectrometer (TJA X-series ICP-MS). During the entire procedure, the Chinese reference standard GBW 04435 (HLP molybdenite) was used to estimate accuracy and precision. The procedural blanks and standard deviation for Re and common Os are 2.2 ± 1.1 and 0.7 ± 0.1 pg, respectively.

Results

Re-Os data of 15 samples are shown in Table 2. The stage III disseminated to massive samples have moderate Re and Os concentrations (^{187}Re ranging from 66.87 to 74.40 ppm, and ^{187}Os ranging from 1475.6 to 1638.8 ppb) and model ages range from 1294 ± 19 Ma to 1323 ± 19 Ma with an average of 1306 ± 8 Ma (MSWD = 1.1, n = 6). The stage V spotted-patchy molybdenite in sulfide veins also has low Re and Os concentrations (^{187}Re ranging from 4.34 to 4.94 ppm and ^{187}Os ranging from 66.0 to 80.0 ppb) but variable model ages. The small sample aliquants (1 and 21 mg) yield model ages ranging from 907 ± 14 to 929 ± 13 Ma with an inaccurate average age of 919 ± 140 Ma (MSWD = 5.3, n = 2), whereas the larger sample aliquants (~50 mg) yield identical model ages of 974 ± 14 and 982 ± 14 Ma with an accurate average age of 978 ± 10 Ma (MSWD = 0.62, n = 2). The large error of the average age from the small sample aliquants is due to the decoupling of Re and Os within coarse-grained molybdenite (Stein et al. 2003; Selby and Creaser 2004), whereas the large sample aliquants can overcome decoupling of Re and Os within coarse-grained molybdenite (Selby and Creaser 2004; Stein

Table 2 Re-Os isotope data for molybdenite from the Lala copper deposit

Sample	Paragenesis	Weight (g)	Re (ppm)	2σ	^{187}Re (ppm)	2σ	^{187}Os (ppb)	2σ	Model age (Ma)	2σ
0308-1-1	Stage III Disseminated to massive magnetite-sulfide	0.0011	106.4	0.8	66.87	0.49	1475.6	11.0	1310	19
0308-1-2		0.0012	106.9	0.9	67.25	0.58	1498.5	9.0	1323	19
0308-2-1		0.0052	111.7	1.0	70.21	0.62	1530.4	8.8	1294	19
0308-2-2		0.0051	115.0	0.9	72.31	0.57	1583.4	9.1	1300	18
0308-3		0.0052	114.6	1.0	72.01	0.63	1581.2	9.2	1304	19
0308-4		0.0052	118.4	1.1	74.40	0.68	1638.8	9.4	1308	19
LLM-1	Stage IV Banded magnetite-sulfide	0.0306	97.6	0.8	61.40	0.50	1117.0	3.0	1083	9
LLM-2		0.0320	94.5	0.8	59.40	0.50	1096.0	4.0	1097	11
LLM-3-1		0.0270	88.0	1.0	55.30	0.60	1007.0	3.0	1083	13
LLM-3-2		0.0349	89.3	0.9	56.10	0.60	1026.0	3.0	1088	11
LLM-5		0.0321	93.4	1.0	58.70	0.60	1058.0	3.0	1072	12
LLM-6		0.0362	89.3	1.0	56.10	0.60	1020.0	4.0	1081	13
LLM-7		0.0315	89.6	1.0	56.30	0.60	1035.0	4.0	1093	13
0101-1-1	Stage V Sulfide vein	0.0012	7.9	0.1	4.94	0.04	77.0	0.5	929	13
0101-1-2		0.0210	6.9	0.1	4.34	0.03	66.0	0.6	907	14
0101-2-1		0.0501	7.8	0.1	4.89	0.04	79.9	0.5	974	14
0101-2-2		0.0506	7.7	0.1	4.85	0.04	80.0	0.5	982	14
LL-mol		0.0050	136.8	1.3	86.00	0.80	1432.0	10.0	992	16
LL-mol		0.0048	146.1	1.5	91.90	0.90	1528.0	11.0	991	16
LL-mol		0.0049	137.5	1.5	86.40	0.90	1445.0	10.0	996	16
LL-mol		0.0052	135.5	1.4	85.10	0.90	1431.0	10.0	1000	16
LL-mol		0.0058	127.6	1.3	80.20	0.80	1330.0	10.0	988	16
0102	Stage VI Quartz-carbonate vein	0.0012	119.7	0.8	75.21	0.52	1049.0	7.0	831	12
0103		0.0013	181.1	1.4	113.80	0.90	1592.0	10.0	834	12
0104		0.0027	84.8	0.7	53.31	0.45	755.0	4.0	844	12
0105		0.0017	166.0	1.2	104.30	0.80	1454.0	12.0	831	12
0106		0.0013	156.1	1.2	98.09	0.74	1382.0	9.0	840	12
0107		0.0013	136.1	0.9	85.57	0.59	1197.0	8.0	834	12
0108		0.0012	199.0	1.5	125.10	0.90	1755.0	11.0	836	12
0109-1		0.0012	129.9	0.9	81.67	0.58	1135.0	8.0	829	12
0109-2		0.0017	130.9	1.1	82.27	0.67	1150.0	7.0	833	12
0110		0.0011	196.2	1.6	123.30	1.00	1733.0	11.0	838	12

Model age calculations use the ^{187}Re decay constant of $1.666 \pm 0.005 \times 10^{-11}$ year^{-1} (±0.31%; Smoliar et al. 1996);

Sample numbers with 2 are replicate analyses of samples labeled-1;

The data of stage VI banded magnetite-sulfide ore are from Chen and Zhou (2012), and the data of LL-mol are from Wang et al. (2007a)

2006). The ages of the larger sample aliquants are similar to molybdenite Re-Os ages obtained by Wang et al. (2007a). Thus, combined with molybdenite Re-Os ages reported by Wang et al. (2007a), we recalculate the weighted mean model ages of stage V molybdenite as 988 ± 8 Ma (MSWD = 1.3, n = 7). The stage VI vein samples have high Re and Os concentration (^{187}Re ranging from 53.31 to 125.10 ppm and ^{187}Os ranging from 755.0 to 1755.0 ppb) and model ages ranging from 831 ± 12 to 844 ± 12 Ma with an average of 835 ± 4 Ma (MSWD = 0.66, n = 10) and an isochron age of 830 ± 10 Ma (MSWD = 1.2). We interpret the weighted mean model ages of 1306 ± 8, 988 ± 8, and 835 ± 4 as representing the depositional ages of stage III molybdenite, stage V molybdenite, and stage VI molybdenite, respectively (Fig. 5).

Discussion

Timing of multiple mineralization events at Lala

Our Re-Os data, together with those reported by Wang et al. (2007a), Chen and Zhou (2012) and Song (2014), indicate that there were at least four hydrothermal events in the Lala deposit. The stage III disseminated-massive molybdenite samples yield Re-Os ages of the first ore-forming hydrothermal event (1306 ± 8 Ma), which produced the disseminated to massive molybdenite-chalcopyrite-magnetite ores, and this age overlap with the chalcopyrite Re-Os age of 1290 ± 38 Ma by Zhu and Sun (2013) and with the zircon U-Pb age of early Huili volcanism nearby the Lala deposit (Yin et al. 2011). The stage IV banded molybdenite samples yield Re-Os ages of the second ore-forming hydrothermal event (1086 ± 6 Ma), which produced the banded molybdenite-chalcopyrite ores (Chen and Zhou 2012; Song 2014), and this age is supported by the allanite U-Pb age of 1067 ± 41 Ma (Chen and Zhou 2014) and zircon U-Pb age of the late Huili volcanism (Geng et al. 2007; Yin et al. 2011). The stage V spotted-patchy molybdenite samples define the third ore-forming event (988 ± 8 Ma), which produced the sulfide-quartz veins, and this age is within error of the average molybdenite Re-Os age of 993 ± 7 Ma reported by Wang et al. (2007a). The stage VI veined molybdenite samples define the fourth and barren hydrothermal event (835 ± 4 Ma), which produced the late molybdenite-quartz-carbonate veins. The last molybdenite mineralization was roughly coeval with the metamorphism of the Sibao orogeny (860–815 Ma, Greentree 2007; Yang et al. 2012; Zhou et al. 2014) and REE-U redistribution (880–850 Ma, Chen and Zhou 2014; 824 ± 15 Ma, Song 2014; Chen and Zhou 2015). Overall, the main IOCG mineralization (Fe-Cu) formed in the first and second hydrothermal event, REE mineralization formed in the second hydrothermal event but was redistributed in the fourth hydrothermal event (Chen and Zhou 2015), and Mo mineralization formed at all four hydrothermal events.

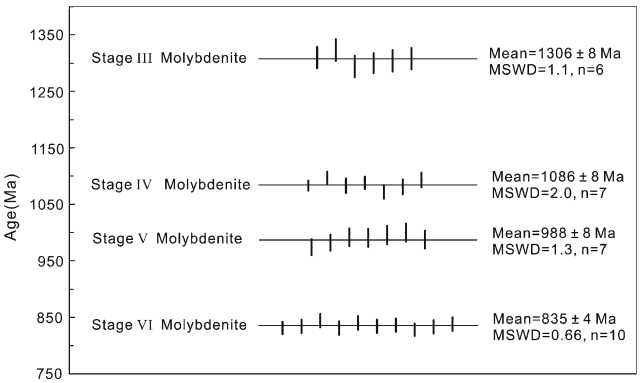

Fig. 5 Weighted averages of Re-Os molybdenite model ages for the Lala deposit. Data of stage IV molybdenite are from Chen and Zhou (2012). Errors are 2σ

Comparison with other IOCG systems

The Fe-Cu deposits in the Kangdian Copper Belt display extensive Na-Ca-K alteration and local brecciation and contain low-Ti iron oxides (magnetite and hematite) and chalcopyrite as primary minerals, with economic Au, Ag, Co, U, and REE by-products (Greentree 2007; Zhao and Zhou 2011). These features are in common with other typical IOCG deposits worldwide (Williams et al. 2005; Groves et al. 2010; Porter 2010). However, the precise timing of the IOCG ore-forming processes in the Kangdian Copper Belt were unclear. Recently, some scientists used Re-Os and U-Pb isotopes to precisely date the hydrothermal events of the Kangdian Copper Belt. Zhao et al. (2013) reported molybdenite Re-Os ages of 1654 ± 7 Ma for magnetite ores, and molybdenite Re-Os ages of 1451 ± 6 Ma for hydrothermal veins from the Yinachang deposit. Hou et al. (2015) obtained a chalcopyrite Re-Os age of 1648 ± 14 Ma for Cu-Fe ores from the Yinachang deposit. Li and Zhou (2015) reported a monazite U-Pb age of 842 ± 9 Ma for REE ores from the Yinachang deposit. Song (2014) obtained a magnetite Re-Os age (ca. 1325 Ma) for magnetite ores and chalcopyrite Re-Os age of 1083 ± 45 Ma for copper ores from the Dahongshan deposit. Zhao et al. (2017) reported a hydrothermal zircon U-Pb age of 1653 ± 18 Ma for stockwork chalcopyrite-magnetite ore, a pyrite Re-Os age of 1026 ± 22 Ma for discordant quartz-carbonate-sulfide veins, and a Re-Os age of 830 Ma for molybdenite within foliated meta-arenite. Zhou et al. (2014) argued that the Kangdian IOCG province may have undergone three mineralization events at 1.66, 1.45, and 1.05 Ga and one post-ore tectonothermal event in the Neoproterozoic (~780–870 Ma).

Our new data record four hydrothermal events in the Lala deposit. Therefore, there were five hydrothermal events in the Kangdian Copper Belt, including three main mineralization events at 1.65, 1.30, and ~1.09–0.99 Ga and two less

important or local hydrothermal/mineralization overprint events at 1.45 and 0.83 Ga (Fig. 6).

Although Hitzman et al. (1992) initially proposed that the most of the sulfide ore postdated Fe oxide formation associated with regional sodic alteration for many IOCG deposits, precise geochronological data for multiple episodes of mineralization were not available until recent studies in some IOCG provinces, e.g., the Fennoscandian Shield (Smith et al. 2009), the Central Andes (Chen 2010), and the Mount Isa Inlier (Duncan et al. 2011). Furthermore, precise U-Pb ages of hydrothermal zircon from four IOCG deposits at Lyon Mountain Granite, Adirondack Highlands in New York State, show that Fe mineralization was episodic (Valley et al. 2009). More recently, Re-Os isotopic data demonstrate that the Cu mineralization may also have formed from multiple hydrothermal episodes, and some IOCG provinces even formed over large intervals of 100 My or more (e.g., Mount Isa Inlier, Duncan et al. 2011; Kangdian, Zhou et al. 2014; Carajás, Moreto et al. 2015a, b). Our Re-Os molybdenite dates, together with previously reported data, provide robust evidence for the multiple nature of hydrothermal mineralization at the Lala deposit. These age data also indicate that young Neoproterozoic hydrothermal events possibly produced local but potentially important Mo-U-REE mineralization.

Possible link between mineralization and supercontinent cycles

The formation of some ore deposits related to convergent and collisional processes (e.g., orogenic Au, volcanic-hosted massive sulfide, Mississippi Valley-type Pb-Zn, epithermal Au-Ag, porphyry deposits) correlates well with the assembly of supercontinents (Cawood and Hawkesworth 2015), whereas others relate to intra-continental settings and divergent margins (e.g., diamond, Ni-Cu-PGE, and sediment-hosted stratiform Cu deposits) during the breakup of supercontinents (Groves and Bierlein 2007). Most IOCG deposits are located in intra-continental settings and/or divergent margins and may

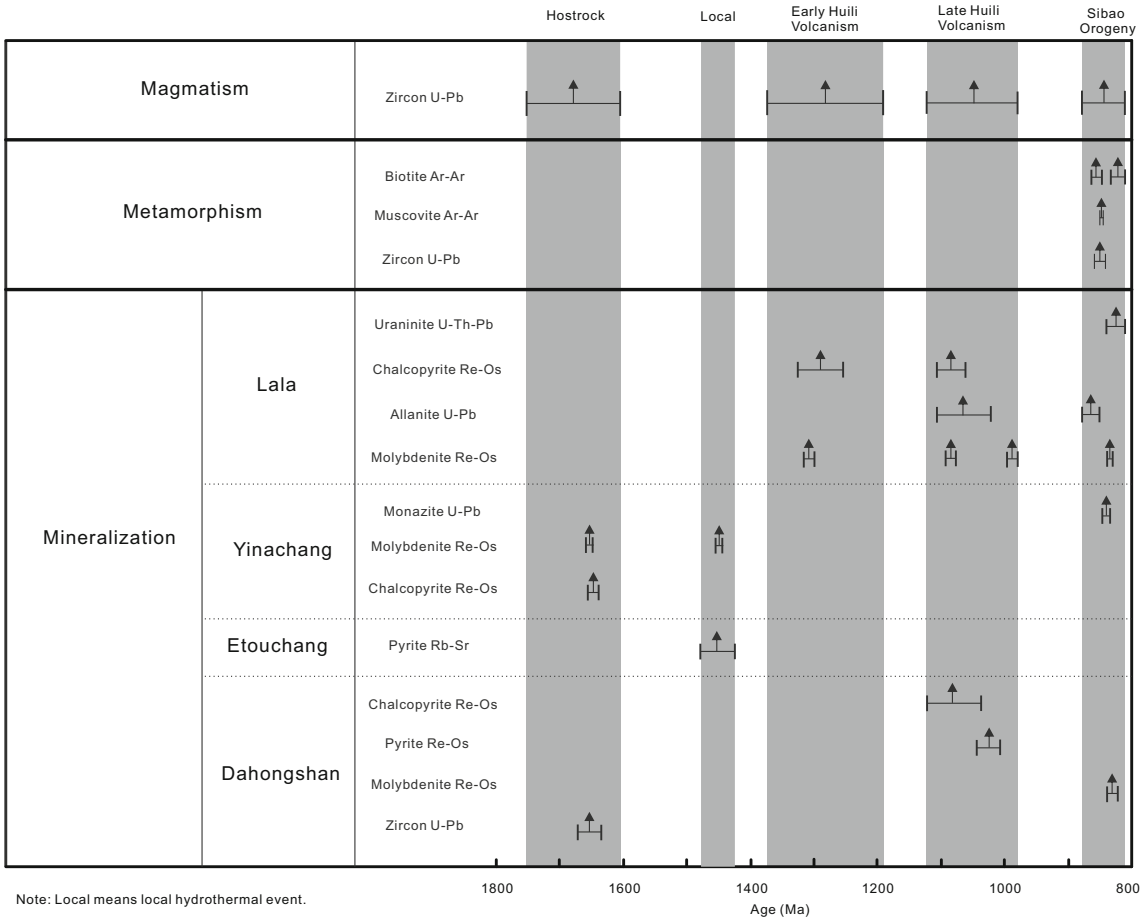

Fig. 6. Summary of geochronological data showing the timing of magmatism, metamorphism, hydrothermal events, and mineralization for the Kangdian Copper Belt (zircon U-Pb: Zhou, et al. 2002; Geng et al. 2007; Yin et al. 2011; Wang et al. 2012; Yang et al. 2012; Chen et al. 2013b; Zhu et al. 2013; Chen et al. 2014; Song 2014; Zhao et al. 2017, and our unpublished data; chalcopyrite Re-Os: Zhu and Sun 2013; Song 2014; Hou et al. 2015; pyrite Re-Os: Zhao et al. 2017; molybdenite Re-Os: Wang et al. 2007a; Chen and Zhou 2012; Zhao et al. 2013, 2017, and this study; allanite U-Pb: Chen and Zhou 2014; monazite U-Pb: Li and Zhou 2015; pyrite Rb-Sr: Zhao et al. 2013; uraninite U-Th-Pb: Song 2014; biotite and muscovite Ar-Ar: Greentree 2007; Zhou et al. 2014)

have formed in extensional settings (Hitzman et al. 1992). Therefore, IOCG deposits may also be correlated with the breakup of supercontinents (Porter 2010; Chen et al. 2013a). Groves et al. (2010) further suggest that the formation of giant Precambrian IOCG deposits was related to extensive mantle underplating that impacted on buoyant metasomatized subcontinental lithospheric mantle. Consequently, the underplate and associated high-temperature metamorphism and magmatism acted both as heat engines, driving fluid circulation over large volumes of the crust, and as ore-forming fluid and metal sources during the breakup of supercontinents (Porter 2010).

The Nuna (or Columbia) supercontinent consolidated at 2.2–1.8 Ga, stabilized at 1.8–1.6 Ga, then fragmented from 1.6 Ga to 1.2 Ga, and eventually broke up at 1.0 Ga (Bradley 2011; Kaur and Chaudhri 2014; Pehrsson et al. 2015; Condie et al. 2015). Cawood and Hawkesworth (2015) point out that the timing of Mesoproterozoic IOCG deposits corresponds with the breakup of Nuna (1.6–1.0 Ga) but not with the assembly of Rodinia (1.3–1.0 Ga). The Mesoproterozoic IOCG deposits include Swan in Cloncurry (1.35 Ga, Duncan et al. 2011), Boss-Bixby in SE Missouri (1.45 Ga, Porter 2010), and Blackbird in the Idaho cobalt belt (ca.1.37 Ga, Aleinikoff et al. 2012). It is generally accepted that the Yangtze Block was part of the Nuna supercontinent (Zhu et al. 2013; Chen et al. 2013b; Zhou et al. 2014). The ~1.65–1.00 Ga IOCG mineralization (see compilation in Fig. 6) may provide evidence for a temporal link between the formation of these IOCG deposits in the Kangdian Copper Belt and the breakup of the Nuna supercontinent. At least four pieces of evidence also show that the western margin of the Yangtze Block was located in an extensional rift setting during the late Paleoproterozoic-Mesoproterozoic as follows: (1) the western margin of the Yangtze Block flanks the Yangtze continent and is underlain by a continental basement (Li et al. 1988; Zhou et al. 2014); (2) the geochemistry of the Mesoproterozoic (~1.7–1.0 Ga) mafic-felsic igneous rocks shows features of intra-continental rift magmatism (Geng et al. 2007; Yin et al. 2011; Chen et al. 2013b, 2014); (3) the sedimentary rocks of the Hekou, Dahongshan, Huili, Julin, and Kunyang Groups (~1.7–1.0 Ga) were deposited in a rifted passive margin (Li et al. 1988; Zhao et al. 2011); and (4) there are many stratiform sediment-hosted Cu deposits formed in the Mesoproterozoic (Tangdan: 1432 ± 19 Ma, Huang et al. 2013; Heiqing: 1359 ± 15 Ma, our unpublished data).

Conclusions

We identify four hydrothermal events in the Lala deposit. The main IOCG mineralization formed in two stages in the Mesoproterozoic at 1.30 to 1.09 Ga, respectively, and local hydrothermal events overprinted the Fe-Cu ores at 0.99 and 0.83 Ga. Our results also indicate that the Lala deposit formed from multiple, protracted hydrothermal events over several hundred million years. The first three Mesoproterozoic mineralization events are related to intra-continental rifting and suggest a link between IOCG mineralization in the Kangdian IOCG metal province and breakup of the supercontinent Nuna; the last Neoproterozoic hydrothermal event is related to the Sibao orogeny which culminated with the amalgamation of the Yangtze Block with the Cathaysia Block.

Acknowledgments This work was supported by National Natural Science Foundation of China (41102044) and Sichuan Youth Science & Technology Foundation of China (2012JQ0026). We thank the Lala copper mining staff, especially Huaijun Zhao and Fuquan Liu for the assistance in the field. We also thank Dr. Wei Chen for sharing the photograph of banded Cu-Mo ore and Dr. Yang Li, Dr. Rongqing Zhang, and Dr. Kongyang Zhu for the help with the preparation of this manuscript. We are grateful to Chris Lawley and three anonymous reviewers for their constructive and incisive comments, which substantially improved the presentation of this paper. Finally, Prof. Bernd Lehmann is gratefully acknowledged for his editorial handling.

References

Aleinikoff JN, Slack JF, Lund K, Evans KV, Fanning CM, Mazdab FK, Wooden JL, Pillers RM (2012) Constraints on the timing of Co-Cu ± Au mineralization in the Blackbird district, Idaho, using SHRIMP U-Pb ages of monazite and xenotime plus zircon ages of related Mesoproterozoic orthogneisses and metasedimentary rocks. Econ Geol 107:1143–1175

Barton MD (2014) Iron oxide(−-Cu-Au-REE-P-Ag-U-Co) systems. Treatise on Geochemistry (2nd Edition) 13:515–541

Bradley DC (2011) Secular trends in the geologic record and the supercontinent cycle. Earth Sci Rev 108:16–33

Cawood PA, Hawkesworth CJ (2015) Temporal relations between mineral deposits and global tectonic cycles, in Jenkin G.RT, Lusty PAJ, Mcdonald I, Smith MP, Boyce AJ, Wilkinson JJ, eds., Ore Deposits in an Evolving Earth. Geological Society of London Special Publications 393: 9–21

Chen HY (2010) Mesozoic IOCG mineralization in the central Andes: an updated review. In: Porter TM (ed) Hydrothermal iron oxide copper-gold and related deposits: a global perspective 3. PGC Publishing, Adelaide, pp 259–272

Chen WT, Zhou MF (2012) Paragenesis, stable isotopes, and Molybdenite Re-Os isotope age of the Lala iron-copper deposit, Southwest China. Econ Geol 107:459–480

Chen WT, Zhou MF (2014) Ages and compositions of primary and secondary allanite from the Lala Fe–Cu deposit, SW China: implications for multiple episodes of hydrothermal events. Contrib Mineral Petrol 168:1043

Chen WT, Zhou MF (2015) Mineralogical and geochemical constraints on mobilization and mineralization of rare earth elements in the Lala Fe-Cu-(Mo, REE) deposit, SW China. Am J Sci 315:671–711

Chen HY, Cooke DR, Baker MJ (2013a) Mesozoic iron oxide copper-gold mineralization in the central Andes and the Gondwana Supercontinent breakup. Econ Geol 108:37–44

Chen WT, Zhou MF, Zhao XF (2013b) Late Paleoproterozoic sedimentary and mafic rocks in the Hekou area, SW China: implication for the reconstruction of the Yangtze Block in Columbia. Precambrian Res 231:61–77

Chen WT, Sun WH, Wang W, Zhao JH, Zhou MF (2014) "Grenvillian" intra-plate mafic magmatism in the southwestern Yangtze Block, SW China. Precambrian Res 242:138–153

Condie K, Pisarevsky SA, Korenaga J, Gardoll S (2015) Is the rate of supercontinent assembly changing with time? Precambrian Res 259: 278–289

De Haller A, Corfu F, Fontboté L, Schaltegger U, Barra F, Chiaradia M, Martin F, Alvarado JZ (2006) Geology, geochronology, and Hf and Pb isotope data of the Raúl-Condestable iron oxide-copper-gold deposit, central coast of Peru. Econ Geol 101:281–310

Du AD, Wu SQ, Sun DZ, Wang SX, Qu WJ, Markey RJ, Stein HJ, Morgan JW, Malinovskiy D (2004) Preparation and certification of Re-Os dating reference materials: molybdenite HLP and JDC. Geostandard and Geoanalytical Research 28:41–52

Duncan RJ, Stein HJ, Evans KA, Hitzman MW, Nelson EP, Kirwin DJ (2011) A new geochronological framework for mineralization and alteration in the Selwyn-Mount Dore Corridor, Eastern Fold Belt, Mount Isa Inlier, Australia: genetic implications for iron oxide copper-gold deposits. Econ Geol 106:169–192

Geng Y, Yang C, Du L, Wang X, Ren L, Zhou X (2007) Chronology and tectonic environment of the Tianbaoshan formation: new evidence from zircon SHRIMP U-Pb age and geochemistry. Geological Review 53:556–563

Greentree MR (2007) Tectonstratigraphic analysis of the Proterozoic Kangdian iron oxide–copper province, south west China. Ph.D. Thesis, University of Western Australia: 284

Greentree MR, Li ZX (2008) The oldest known rocks in south-western China: SHRIMP U–Pb magmatic crystallisation age and detrital provenance analysis of the Paleoproterozoic Dahongshan Group. J Asian Earth Sci 33:289–302

Greentree MR, Li ZX, Li XH, Wu H (2006) Late Mesoproterozoic to earliest Neoproterozoic basin record of the Sibao orogenesis in western South China and relationship to the assembly of Rodinia. Precambrian Res 151:79–100

Groves DI, Bierlein FP (2007) Geodynamic settings of mineral deposit systems. J Geol Soc Lond 164:19–30

Groves DI, Bierlein FP, Meinert LD, Hitzman MW (2010) Iron oxide copper–gold (IOCG) deposits through Earth history: implications for origin, lithospheric setting, and distinction from other epigenetic iron oxide deposits. Econ Geol 105:641–654

Hitzman MW, Valenta RK (2005) Uranium in iron oxide-copper–gold (IOCG) systems. Econ Geol 100:1657–1661

Hitzman MW, Oreskes N, Einaudi MT (1992) Geological characteristics and tectonic setting of Proterozoic iron oxide (cu-U-au-REE) deposit. Precambrian Res 58:241–287

Hou L, Ding J, Deng J, Peng HJ (2015) Geology, geochronology, and geochemistry of the Yinachang Fe–Cu–Au–REE deposit of the Kangdian region of SW China: evidence for a Paleo–Mesoproterozoic tectono-magmatic event and associated IOCG systems in the western Yangtze Block. J Asian Earth Sci 103:129–149

Huang XW, Zhao XF, Qi L, Zhou MF (2013) Re-Os and S isotopic constraints on the origins of two mineralization events at the Tangdan sedimentary rock-hosted stratiform Cu deposit, SW China. Chem Geol 347:9–19

Kaur P, Chaudhri N (2014) Metallogeny associated with the Palaeo-Mesoproterozoic Columbia supercontinent cycle: a synthesis of major metallic deposits. Ore Geol Rev 56:415–422

Li XC, Zhou MF (2015) Multiple stages of hydrothermal REE remobilization recorded in fluorapatite in the Paleoproterozoic Yinachang Fe–Cu–(REE) deposit, Southwest China. Geochim Cosmochim Acta 166:53–73

Li FH, Qin JM, Shen YL, Yu FX, Zhou GF, Pan XN, Li XZ (1988) The Presinian in the Kangdian area. Chongqing Publishing House, Chongqing, pp 1–396

Li ZX, Zhang L, Powell CM (1995) South China in Rodinia: part of the missing link between Australia–East Antarctica and Laurentia? Geology 23:407–410

Li ZX, Li XH, Zhou H, Kinny PD (2002) Grenvillian continental collision in south China: new SHRIMP U–Pb zircon results and implications for the configuration of Rodinia. Geology 30:163–166

Moreto CPN, Monteiro LVS, Xavier RP, Creaser RA, DuFrane A, GHC M, Silva MAD, Tassinari CCG, Sato K (2015a) Timing of multiple hydrothermal events in the iron oxide–copper–gold deposits of the Southern Copper Belt, Carajás Province, Brazil. Mineral Deposita 50:517–546

Moreto CPN, Monteiro LVS, Xavier RP, Creaser R, Dufrane A, Tassinari CG, Sato K, Kemp AIS, Amaral WS (2015b) Neoarchean and Paleoproterozoic iron oxide-copper-gold events at the Sossego deposit, Carajás Province, Brazil: Re-Os and U-Pb geochronological evidence. Econ Geol 110:809–835

Pehrsson SJ, Eglington BM, Evans DAD, Huston D, Reddy SM (2015) Metallogeny and its link to orogenic style during the Nuna supercontinent cycle, in Li ZX, Evans DAD, Murphy JB, eds., Supercontinent Cycles Through Earth History. Geological Society of London Special Publications 424: 83–94

Porter TM (2010) Advances in the understanding of IOCG and related deposits. In: Porter TM (ed) Hydrothermal iron oxide copper-gold and related deposits: a global perspective 3. PGC Publishing, Adelaide, pp 5–106

Requia K, Stein H, Fontbote L, Chiaradia M (2003) Re-Os and Pb-Pb geochronology of the Archean Salobo iron oxide copper-gold deposit, Carajas mineral province, northern Brazil. Mineral Deposita 38:727–738

Selby D, Creaser RA (2004) Macroscale NTIMS and microscale LA-MC-ICP-MS Re–Os isotopic analysis of molybdenite: testing spatial restrictions for reliable Re–Os age determinations, and implications for the decoupling of Re and Os within molybdenite. Geochim Cosmochim Acta 68:3897–3908

Sillitoe RH (2012) Copper provinces. Society of Economic Geologists Special Publication 16:1–18

Skirrow RG, Bastrakov EN, Barovich K, Fraser GL, Creaser R, Fanning MC, Raymond OL, Davidson GJ (2007) Timing of iron oxide Cu-Au-(U) hydrothermal activity and Nd isotope constraints on metal sources in the Gawler craton, South Australia. Econ Geol 102:1441–1470

Smith MP, Storey CD, Jeffries TE, Ryan C (2009) In situ U–Pb and trace element analysis of accessory minerals in the Kiruna district, Norrbotten, Sweden: new constraints on the timing and origin of mineralization. J Petrol 50:2063–2094

Smoliar MI, Walker RJ, Morgan JW (1996) Re-Os ages of group IIA, IIIA, IVA, and IVB iron meteorites. Science 271:1099–1102

Song H (2014) Precambrian copper-iron-gold-uranium ploymetallic deposits and their regional metallogey in southwestern margin of Yangtze Block. Ph.D thesis, The Chengdu University of Technology: 1–217

Stein HJ (2006) Low-rhenium molybdenite by metamorphism in northern Sweden: recognition, genesis, and global implications. Lithos 87: 300–327

Stein HJ (2014) Dating and tracing the history of ore formation. Treatise on geochemistry (2nd Edition) 13:87–118

Stein HJ, Markey RJ, Morgan JW, Hannah JL, Scherstén A (2001) The remarkable Re-Os chronometer in molybdenite: how and why it works. Terra Nov. 13:479–486

Stein H, Schersten A, Hannah J, Markey R (2003) Sub-grain scale decoupling of Re and ^{187}Os and assessment of laser ablation ICP-MS spot dating in molybdenite. Geochim Cosmochim Acta 67: 3673–3686

Valley PM, Hanchar JM, Whitehouse MJ (2009) Direct dating of Fe oxide-(Cu-Au) mineralization by U/Pb zircon geochronology. Geology 37:223–226

Wang DH, Luo YN, Qu WJ, Li YQ, Fu DM, Li YG, Li CJ, Chen ZY, Fu XF (2007a) Geology, geochemistry and exploration of PGE deposits in SW China. Geological Publishing House, Beijing, pp 1–335

Wang XL, Zhou JC, Griffin WL, Wang RC, Qiu JS, O'Reilly SY, Xu XS, Liu XM, Zhang GL (2007b) Detrital zircon geochronology of Precambrian basement sequences in the Jiangnan orogen: dating the assembly of the Yangtze and Cathaysia blocks. Precambrian Res 159:117–131

Wang Z, Zhou B, Guo Y, Yang B, Liao Z, Wang S (2012) Geochemistry and zircon U–Pb dating of Tangtang granite in the western margin of the Yangtze Platform. Acta Petrol Mineral 31:652–662

Williams PJ, Barton MD, Johnson DA, Fontboté L, de Haller A, Mark G, Oliver NHS, Marschik R (2005) Iron oxide copper-gold deposits: Geology, Space-time distribution, and possible modes of origin. Economic Geology 100th Anniversary Volume: 371–405

Yan DP, Zhou MF, Song HL, Wang XW, Malpas J (2003) Origin and tectonic significance of a Mesozoic multi-layer over-thrust within the Yangtze Block (South China). Tectonophysics 361:239–254

Yang H, Liu FL, Du LL, Liu PH, Wang F (2012) Zircon U-Pb dating for metavolcanites in the Laochanghe Formation of the Dahongshan Group in southwestern Yangtze Block, and its geological significance. Acta Petrol Sin 28:2994–3014

Yao JL, Shu LS, Santosh M, Zhao GC (2014) Neoproterozoic arc-related mafic–ultramafic rocks and syn-collision granite from the western segment of the Jiangnan Orogen, South China: constraints on the Neoproterozoic assembly of the Yangtze and Cathaysia Blocks. Precambrian Res 243:39–62

Yin FG, Sun ZM, Zhang Z (2011) Mesoproterozoic stratigraphicstructure framework in Huili-Dongchuan area. Geological Review 57:770–778

Zhao GC (2015) Jiangnan Orogen in South China: developing from divergent double subduction. Gondwana Res 27:1173–1180

Zhao GC, Cawood PA (2012) Precambrian geology of China. Precambrian Res 222:13–54

Zhao XF, Zhou MF (2011) Fe-Cu deposits in the Kangdian region, SW China: a Proterozoic IOCG (iron-oxide-copper-gold) metallogenic province. Mineral Deposita 46:731–747

Zhao XF, Zhou MF, Li JW, Sun M, Gao JF, Sun WH, Yang JH (2010) Late Paleoproterozoic to early Mesoproterozoic Dongchuan Group in Yunnan, SW China: Implications for tectonic evolution of the Yangtze Block. Precambrian Res 182(1–2):57–69

Zhao JH, Zhou MF, Yan DP, Zheng JP, Li JW (2011) Reappraisal of the ages of Neoproterozoic strata in South China: no connection with the Grenvillian orogeny. Geology 39:299–302

Zhao XF, Zhou MF, Li JW, Selby D, Li XH, Qi L (2013) Sulfide Re-Os and Rb-Sr isotopic dating of the Kangdian IOCG metallogenic province, SWChina: implications for regional metallogenesis. Econ Geol 108:1489–1498

Zhao XF, Zhou MF, Su ZK, Li XC, Chen WT, Li JW (2017) Geology, geochronology, and geochemistry of the Dahongshan Fe-Cu-(Au-Ag) deposit, Southwest China: implications for the formation of iron oxide copper-gold deposits in intracratonic rift settings. Econ Geol 112:603–628

Zhou MF, Yan DP, Kennedy AK, Li Y, Ding J (2002) SHRIMP U–Pb zircon geochronological and geochemical evidence for Neoproterozoic arc-magmatism along the western margin of the Yangtze Block, South China. Earth Planet Sci Lett 196: 51–67

Zhou MF, ZhaoXF CWT, Li XC, Wang W, Yan DP, Qiu HN (2014) Proterozoic Fe-Cu metallogeny and supercontinental cycles of the southwestern Yangtze Block, southern China and northern Vietnam. Earth Sci Rev 139:59–82

Zhu ZM (2016) Gold in iron oxide copper–gold deposits. Ore Geol Rev 72:37–42

Zhu ZM, Sun YL (2013) Direct Re-Os dating of chalcopyrite from the Lala IOCG deposit in the Kangdian Copper Belt. China: Economic Geology 108:871–882

Zhu ZM, Zeng LX, Zhou JY, Luo LP, Chen JB, Shen B (2009) Lala iron oxide-copper-gold deposit in Sichuan Province: evidences from mineralography. Geol J China Univ 15:485–495

Zhu ZM, Hou KJ, Zhu KY, Tan HQ (2013) Geochronology and geochemistry of the Hekou Group in Sichuan Province, SW China. Geochem J 47:51–64